Structural Insight into G-Protein Coupled Receptor Binding by Apelin[†]

David N. Langelaan,[‡] E. Meghan Bebbington,[‡] Tyler Reddy,[‡] and Jan K. Rainey*[,‡,§]

Departments of Biochemistry & Molecular Biology and Chemistry, Dalhousie University, Halifax, Nova Scotia B3H 1X5 Canada

Received October 2, 2008; Revised Manuscript Received December 10, 2008

ABSTRACT: Apelin peptides are the cognate ligands for the G-protein coupled receptor APJ, with functions in the cardiovascular and central nervous systems, in glucose metabolism and as a human immunodeficiency virus (HIV-1) coreceptor. Apelin is found in 13−36 residue forms *in vivo*. The structures of five isoforms of apelin at physiological versus low (5−6 °C) temperature are compared here using circular dichroism (CD) and nuclear magnetic resonance (NMR) spectroscopy, demonstrating increased structure at low temperature. Far-ultraviolet (UV) CD spectra are predominantly random coil for apelin isoforms, but are convoluted by unusual bands from the C-terminal phenylalanine side chain. These bands, assigned using F13A-apelin-13, are accentuated at 5 °C and imply conformational restriction. At 35 °C, the R6−L9 region of apelin-17 is well structured, consistent with previous mutagenesis results showing necessity of this segment for apelin−APJ binding and activation. At 5 °C, R6−L9 retains its structuring while the functionally critical C-terminal G13−F17 region also becomes highly structured. Type IV β-turns and some polyproline-II structure alongside F17 side chain motional reduction correlate well with CD spectral properties. *Cis*−*trans* peptide bond isomerization at P14 and P16 produces two sequentially assignable conformers (both *trans*:both *cis* ∼4:1) alongside less populated conformers. Chemical shift assignment of apelin-12, -13 and pyroglutamate-apelin-13 implies highly similar structuring and the same isomerization at the C-terminus. Based on the apelin-17 structure, a two-step binding and activation mechanism is hypothesized.

The apelin family of peptides (*1*) are the cognate ligands to the class A rhodopsin-like G-protein coupled receptor (GPCR[1]) named APJ (*2*). Apelin is expressed as a 77 amino acid long preproprotein and is cleaved intracellularly to produce a number of secreted bioactive peptides 13−36 residues in length (Table 1), all of which retain the C-terminus of the preproprotein (*1*). Activation of APJ by apelin results in downstream effects on the cardiovascular and central nervous systems as well as in the adipoinsular axis. Apelin is among the most potent of identified inotropic agents, increasing muscle contractility with an EC_{50} (half-maximal effective concentration) of ∼33 pmol/L in rat heart (*3*). Adipocytes produce apelin and APJ (*4*), and there is a correlation between plasma levels of apelin and obesity in humans (*4, 5*) and mice (*4*). Similarly, apelin upregulation is observed in conjunction with an elevated body mass index (*5*). Human immunodeficiency virus (HIV-1) uses APJ as a coreceptor for CD4-mediated viral fusion to host cells (reviewed in ref *6*). Recent studies have shown that apelin induces neoangiogenesis during tumor formation (*7, 8*), and APJ knockout mice have diminished atherosclerotic lesions despite lacking apolipoprotein-E, suggesting a role for APJ signaling in atherosclerotic plaque deposition (*9*). Given its involvement in key physiological and disease processes, the apelin−APJ system is a promising target for therapeutics. Small molecule (*6*) and peptide (*10*) based drug design will be facilitated by high-resolution structures for apelin and APJ, neither of which was available prior to this work.

The fact that apelin peptides (Table 1) having at least the 12 C-terminal residues are highly specific ligands for APJ (*6, 11, 12*) suggests a specific structuring to allow the peptide-GPCR recognition and binding events that lead to APJ activation. However, apelin-13 and apelin-36 adopt a "random conformation" based on studies by electronic

[†] Supported by startup funding from Dalhousie University, a Natural Sciences and Engineering Research Council of Canada (NSERC) Discovery Grant, a Dalhousie University Faculty of Medicine Intramural Grant, a grant from the E. Gordon Young Endowment Fund, and New Investigator Fee Waivers from the Canadian National High-Field NMR Centre (NANUC); D.N.L. and T.R. are current Canada Graduate Scholarship recipients from NSERC, and E.M.B. was a recipient of an NSERC Undergraduate Student Research Award. Operation of Atlantic Region Magnetic Resonance Centre is funded by NSERC and Dalhousie University; operation of NANUC is funded by the Canadian Institutes of Health Research, NSERC, and the University of Alberta.

* Corresponding author: Dr. Jan Rainey, Department of Biochemistry & Molecular Biology and Department of Chemistry, Dalhousie University, Tupper Medical Building, Room 10-N1, 5850 College St., Halifax, NS B3H 1X5 Canada. Phone: (902) 494-4632. Fax: (902) 494-1355. E-mail: jan.rainey@dal.ca.

[‡] Department of Biochemistry & Molecular Biology.

[§] Department of Chemistry.

[1] Abbreviations: CD, electronic circular dichroism; COSY, correlation spectroscopy; DIPSI, decoupling in the presence of scalar interactions; DMF, *N*,*N*-dimethylformamide; DQF-COSY, double-quantum filtered COSY; DSS, 2,2-dimethyl-2-silapentane-5-sulfonate; Fmoc, 9-fluorenylmethoxycarbonyl; GPCR, G-protein coupled receptor; HBTU, *O*-benzotriazole-*N*,*N*,*N*′,*N*′-tetramethyl-uronium-hexafluoro-phosphate; HIV-1, human immunodeficiency virus 1; HPLC, high performance liquid chromatography; HSQC, heteronuclear single quantum coherence; $^3J_{HNH\alpha}$, 3-bond *J*-coupling constant between subscripted nuclei; MALDI-MS, matrix assisted laser desorption ionization mass spectrometry; NMR, nuclear magnetic resonance; NOE, nuclear Overhauser effect; NOESY, NOE spectroscopy; PP_{II}, polyproline-II; Pyr, pyroglutamate; rmsd, root-mean-square deviation; RP-HPLC, reversed phase HPLC; TOCSY, total correlation spectroscopy; UV, ultraviolet.

10.1021/bi801864b CCC: $40.75
Published on Web 01/05/2009

circular dichroism (CD) spectroscopy (*13*). However, two types of secondary structure potentially consistent with these CD spectra have been identified in the literature. First, it has been hypothesized that β-turns are ubiquitous and important for GPCR binding peptides (*14*). Second, polyproline-II (PP_{II}) is often found in short "unstructured" peptide ligands (*15*), and is postulated to play a critical role in intermolecular interactions (*16*). The CD study by Fan et al. was conducted at ambient temperature, and it is reasonable to expect that a short peptide at ambient or physiological temperature will be free to undergo a great deal of conformational sampling (*17*).

Nuclear magnetic resonance (NMR) spectroscopy is an ideal method for studying the structure and dynamics of small peptides such as apelin (*17, 18*). The final structural ensemble generated for peptides or proteins will often contain several different conformations, each of which may be important in some aspect of function (*19*). To tease out peptide conformation(s) relevant to receptor binding, a favored strategy is the use of lowered temperature (0−8 °C) to allow increased sampling of entropically disfavored states through reduction of the entropic contribution to Gibbs free energy, i.e., $T\Delta S$ in $\Delta G = \Delta H - T\Delta S$ (*18, 20, 21*). Perhaps logically, decreasing temperature has recently been shown to affect the dynamics of intrinsically disordered peptides differently than peptides that have inherent structuring accentuated by low temperature. Specifically, NMR spectroscopy showed inherently structured regions of peptides to have decreased motion in comparison to intrinsically disordered peptides (*22*). Isolated peptidic ligands at low temperature have been shown to adopt the same structure as the bound state (*23*), and a number of peptides activating the chemokine GPCR CXCR4 show the same structuring at low temperature (*21*). In this manuscript, NMR and CD spectroscopy results are presented for a variety of apelin peptides at both physiological and low temperatures allowing determination of the bioactive structure of apelin. These results are placed into a functional context through correlation with previous studies.

EXPERIMENTAL PROCEDURES

Materials. 9-Fluorenylmethoxycarbonyl (Fmoc) protected amino acids, Fmoc-Phe-Wang resin (100−200 mesh, 0.49 mmol/g loading) and O-benzotriazole-*N*,*N*,*N*′,*N*′-tetramethyl-uronium-hexafluoro-phosphate (HBTU) were obtained from AAPPTec (Louisville, KY). Side chain protecting groups on Fmoc amino acids were 2,2,4,6,7-pentamethyldihydrobenzofuran (Pbf) for Arg; triphenylmethane (Trt) for Gln and His; *tert*-butyl (tBu) for Ser; and *tert*-butoxycarbonyl (Boc) for Lys. *N*,*N*-Dimethylformamide (DMF, sequencing grade) was obtained from Fisher Scientific (Ottawa, ON). Pyroglutamate modified apelin-13, F13A-apelin-13 and apelin-36 (>95% purity) were obtained from AnaSpec (San Jose, CA). Deuterium oxide (D_2O; 99.8 atom % D) and D_2O containing 1% (w/w) sodium 2,2-dimethyl-2-silapentane-5-sulfonate (DSS) were obtained from C/D/N isotopes (Pointe-Claire, QC). All other chemicals were obtained at biotechnology, high performance liquid chromatography (HPLC) or reagent grade, as appropriate, from Sigma Aldrich (Oakville, ON).

Peptide Synthesis and Purification. Apelin-12, -13 and -17 (Table 1) were produced in multimilligram quantities using standard Fmoc-based solid-phase peptide synthesis protocols (*24*). An automated peptide synthesizer (AAPPTec Endeavor 90) was used to perform all synthetic steps prior to peptide-resin cleavage. Fmoc-Phe-Wang resin provided a C-terminal Phe residue with free carboxy terminus. Briefly, each Fmoc-amino acid was double-coupled in DMF using HBTU and *N*,*N*-diisopropylethylamine preactivation, Fmoc deprotection was performed using excess piperidine in DMF and coupling and deprotection were monitored by the Kaiser or isatin tests (*25*), as appropriate. Peptide-resin cleavage and side chain deprotection was carried out in trifluoroacetic acid:phenol: triisoproylsilane:water:ethane dithiol:thioanisole (85:5:2.5: 2.5:2.5:2.5 by volume) at room temperature for 2 h, followed by precipitation and centrifugation (4 × 10 min, 3500 rpm, 0 °C) in chilled *tert*-butyl methyl ether. After lyophilization, each reaction mixture was dissolved in water and examined by analytical reverse phase (RP) HPLC (Beckman System Gold, Fullerton, CA) using a water:acetonitrile (A:B) gradient with B progressing from 2 to 80% on a C_{18} column (5 μm particle, 40 mm × 250 mm Spirit Peptide column, AAPPTec) monitored at 210 nm. A semipreparative C_{18} column (5 μm particle, 100 mm × 250 mm Spirit Peptide column, AAPPTec) with fraction collection (GE-AKTA Frac-920, Piscataway, NJ) was used for purification. Product masses and amino acid composition were confirmed by electrospray ionization mass spectrometry (DalGen Proteomics Core Facility, Halifax, NS) and quantitative amino acid analysis (Alberta Peptide Institute, Edmonton, AB and Hospital for Sick Children, Toronto, ON), respectively (results not shown).

CD Spectroscopy. Far-ultraviolet (UV) CD spectra of peptides were recorded using a Jasco J-810 spectropolarimeter (Easton, MD) with temperature control capability. Solutions of apelin peptides (200 μM; exact concentration determined by quantitative amino acid analysis, Hospital for Sick Children, Toronto, ON) were prepared in 20 mM sodium phosphate buffer adjusted to pH 7.00 ± 0.05 using NaOH and H_2SO_4. The spectra were measured from 260 nm downward in 1 nm steps, with reliable ellipticity values typically observed at >174 nm for apelin solutions based on spectropolarimeter photomultiplier tube voltages. Quartz cuvettes with path length of 0.01 cm (Hellma, Müllheim, Germany) were used. Nine trials were completed for each apelin condition, including buffer blanks. Machine data was converted to mean residue ellipticity [θ], averaged over all trials and blank subtracted followed by sliding-window averaging over 3 nm stretches so that [θ] reported at a given wavelength λ is

$$[\theta] = {}^1\!/_4[\theta]_{\lambda-1} + {}^1\!/_2[\theta]_{\lambda} + {}^1\!/_4[\theta]_{\lambda+1} \quad (1)$$

CD data is provided in the Supporting Information without sliding-window averaging.

NMR Spectroscopy. NMR samples of apelin-12, apelin-13, Pyr-apelin 13 and apelin-17 were prepared with 3−4 mM peptide in a 90% H_2O/10% D_2O mixture with 20 mM $Na^+CD_3COO^-$, 1 mM NaN_3, and 1 mM DSS as an internal standard. Sample pH in all cases was adjusted to 5.00 ± 0.05 using DCl and NaOD. Spectra were acquired at the Atlantic Region Magnetic Resonance Centre (ARMRC, Halifax, NS) on a 500 MHz Bruker AVANCE II spectrometer (Milton, ON) and the National High Field Nuclear Magnetic Resonance Centre (NANUC, Edmonton, AB) on

Table 1: The Sequences of the Bioactive Forms of Human Apelin, as Well as the Functionally Essential Apelin-12 C-Terminal Region (Bolded in Each Peptide Sequence)

apelin-36	H_2N-LVQPRGSRNGPGPWQGGRRKFRRQ**RPRLSHKGPMPF**-COOH
apelin-17	H_2N-KFRRQ**RPRLSHKGPMPF**-COOH
Pyr-apelin-13[a]	HN-Pyr-**RPRLSHKGPMPF**-COOH
apelin-13	H_2N-Q**RPRLSHKGPMPF**-COOH
apelin-12	H_2N-**RPRLSHKGPMPF**-COOH

[a] Pyr represents the amino acid pyroglutamate.

500, 600 and 800 MHz Varian INOVA spectrometers (Palo Alto, CA). The latter is equipped with a cryogenically cooled probe. One-dimensional ^{1}H, natural abundance gradient enhanced ^{13}C−^{1}H HSQC, ^{1}H−^{1}H NOESY (400 ms mixing time), ^{1}H−^{1}H TOCSY (60 ms mixing time with DIPSI spin lock) and double-quantum filtered COSY (DQF-COSY) experiments were acquired for apelin-17 at 5 and 35 °C. Similar sets of experiments were performed for the other peptides except that ^{1}H−^{1}H ROESY (200 ms mixing time) replaced the NOESY experiment, and for apelin-12 and Pyr-apelin-13 spectra were collected at 6 °C instead of 5 °C due to instrumental problems. NMR data was processed using NMRPipe (*26*) and manually assigned in Sparky 3 (T. D. Goddard and D. G. Kneller, University of California, San Francisco).

NMR Structure Calculation and Ensemble Analysis. Peak volumes for NOESY spectra of apelin-17 were estimated using Sparky's integration algorithm with Gaussian lineshapes and no peak motion allowed. For peaks where this algorithm failed, the sum over ellipse method was used. Peak volumes for both Gaussian and sum over ellipse fits were independently calibrated so that the smallest volume represented a 6 Å distance while the largest volume peaks represent a 1.8 Å distance. The python scripting interface of xplor-NIH version 2.18 (*27*) was used for simulated annealing structure calculations, with ambiguous assignments and NOE potential scaling implemented as described previously (*28*). Three apelin-17 structural ensembles were refined and calculated: one for the NMR data at 35 °C and two separate conformers based on the 5 °C data. The two structural ensembles for the 5 °C NMR data were produced using two separate sets of NOEs assignable to apelin-17 conformers in slow conformational exchange in the G13−F17 region. For all cases, NOE restraint refinements were performed through iterative calculation of a number of 100-member structural ensembles, following methods introduced previously (*28*). Briefly, ensembles were analyzed using an in-house tcl/tk script which calculated the magnitude and frequency of violating NOEs. Starting from a violation length of >0.5 Å in >50% of ensemble members, the stringency was gradually increased to a final value of 0.05 Å in 15% (35 °C) or 10% (5 °C) of ensemble members until the average energy of each ensemble reached a consistent minimum (iterative structure calculation statistics shown in Table 2). Ensembles of 200 structures were then calculated, with the 80 lowest energy structures retained for analysis. In addition, simulated annealing of apelin-17 without inclusion of any experimentally derived restraints was used to generate an ensemble of 1000 structures. This was used as a control both for meaningful root-mean-square deviation (rmsd) values of the peptide backbone atoms and for frequency of β-turns in an unrestrained peptide.

For each final ensemble of structures: (i) Procheck-NMR was used to tabulate residues in favored, allowed, generously allowed and disallowed areas of the Ramachandran plot (*29*); (ii) an in-house tcl/tk script was used to determine the residues with dihedral angles corresponding to a PP_{II} conformation (according to (ϕ, ψ) definitions of $-90° \leq \phi \leq -20°$ and $50° \leq \psi \leq 240°$ derived by Best et al. through statistical analysis of the Protein Data Bank (*30*)); and (iii) Promotif-NMR was used to determine frequency and location of β-turns (*31*). The LSQKAB software of the CCP4 suite (*32*) was used to iteratively superpose the clusters over 4−17 residue stretches while an in-house tcl/tk script was used to calculate the rmsd of the backbone atoms within the superposed region (iterative superposition protocol introduced and described in refs *17, 33).* The most converged areas, determined by comparison to rmsds calculated for the ensemble of 1000 unrestrained apelin-17 structures described above, were analyzed for the presence of clustering within the ensemble using Clusterpose (*34*). Rmsd values for each cluster based upon the R1, R2 and R4 methods of Clusterpose (*34*) were parsed into NEXUS format (*35*) by an in-house python script and visualized as phylograms using Figtree (A. Rambaut, University of Edinburgh). A group of structures were considered to be part of the same cluster if (1) the R1, R2 and R4 methods all placed these structures into nearly or exactly the same cluster; (2) the resulting cluster constituted ≥10% of the total ensemble; and (3) the increase in rmsd caused by superposing one cluster onto another is large compared to the rmsd of structures within a cluster. Pymol (Delano Scientific, San Carlos, CA) was used for molecular visualization. Chemical shifts, restraint files, and the final 80-member ensembles for apelin-17 at 35 °C and for conformers A and B of apelin-17 at 5 °C have been deposited at the BioMagResBank (*36*) using SMSDep (BMRB Accession Codes 20029, 20030 and 20031).

RESULTS

CD Spectroscopy of the Apelins. Far-UV CD spectroscopy of all five isoforms of apelin (apelin-12, -13, -17, -36 and Pyr-apelin-13) in phosphate buffer (20 mM, pH 7.00 ± 0.05) showed marked differences between 35 and 5 °C (Figures 1 and S1 in the Supporting Information; detailed spectral analysis in Table S1 of the Supporting Information). At both temperatures, apelin CD spectra show no evidence of α-helical or β-sheet secondary structure, nor are the spectra consistent with a strictly random coil structure (*37*). The differences in spectral properties at 35 and 5 °C are remarkably similar between isoforms (Figures 1 and S1 of the Supporting Information). Specifically, each apelin isoform had greater CD intensity in the ∼210−230 nm wavelength region at 5 °C vs 35 °C, a crossing of the 5 and 35 °C spectra at ∼208−211 nm, and decreased CD at 5 °C vs 35 °C for all wavelengths below the crossover point. A positive band

Table 2: Summary of Iterative Structure Calculation Protocols and Restraints Employed for Production of the 80 Lowest Energy Structures from 200 Calculated for Each of the Three Apelin-17 Ensembles Produced Alongside Structural Statistics, Energies of Converged Structural Ensembles and Violation Occurrences

		5 °C	
	35 °C	conformer A	conformer B
Structure Calculation Parameters[a]			
rounds of NOE refinement prior to ^3J-coupling incorporation	3	6	7
total rounds of NOE refinement	12	37	32
Unique NOE Restraints			
total	285	562	529
intraresidue	146	224	226
sequential	108	222	194
medium range ($i - j \leq 4$)	22	62	54
long range ($i - j > 4$)	0	0	0
ambiguous	9	54	55
^3J-Coupling Restraints			
no. of restraints	10	12	12
Ramachandran Plot Statistics			
core	226	171	150
allowed	457	431	395
generously allowed	86	166	196
disallowed	111	112	139
in PP_{II} conformation (*30*)	280/1500	345/1500	323/1500
no. of type I β-turns	9	0	1
no. of type II β-turns	2	9	2
no. of type IV β-turns	123	96	193
no. of type VIb β-turns	0	0	3
no. of type VIa β-turns	0	0	5
no. of type VIII β-turns	10	0	15
XPLOR-NIH Energies (kcal/mol)[b]			
total	45.14 ± 5.39	53.45 ± 5.34	61.74 ± 6.40
NOE	0.60 ± 0.49	0.67 ± 0.59	0.61 ± 0.62
J coupling	2.55 ± 1.30	1.83 ± 0.88	2.71 ± 1.22
Violations			
NOE violations > 0.5 Å	0	0	0
NOE violations of 0.3−0.5 Å	0	3	0
NOE violations of 0.2−0.3 Å	4	3	7
^3J-coupling violations	11	4	6

[a] Iterative NOE contact refinement was carried out as described previously (*28*) through calculation of the given total number of 100-member ensembles where the initial rounds were performed without ^3J-couplings incorporated. [b] Ranges are given by average deviations for XPLOR-NIH energies.

with maximum at 217−218 nm is obvious at 5 °C in each apelin peptide except apelin-36 and F13A substituted apelin-13 (F13A-apelin-13). The ellipticity for apelin-36 did not become positive in this wavelength range, but the same positive band convolutes its CD spectrum. All apelin spectra show a negative band below 200 nm, but with the exception of apelin-36 and F13A- apelin-13 these are convoluted with a positive band at 194−195 nm.

A positive band at ∼217−230 nm and strong negative band below 200 nm are consistent with PP_{II} structure, however the positive band at 194−195 is not consistent with a PP_{II} structure (*15, 38, 39*). β-Turn structures produce a variety of different spectra (*40*), but they all have inconsistencies with the apelin spectra in Figure 1. Although backbone amide transitions are typically observed in the far-UV region of CD spectra, this region of the spectrum sometimes shows bands from aromatic side chains. In particular, positive bands at 197 nm and 217−220 nm have been attributed to Phe side chains (*41, 42*). Since apelin-12, -13 and Pyr-apelin-13 only have a single aromatic residue (the C-terminal Phe), the appearance of bands from this Phe side chain in apelin CD spectra was tested using F13A substituted apelin-13. Strikingly, the CD spectra of F13A-apelin-13 at both 35 and 5 °C do not have the positive bands at 197 nm or 217−220 nm characteristic of the apelins with a C-terminal Phe (Figures 1 and S1 of the Supporting Information). This is a clear indication that these spectral characteristics are due primarily to this Phe side chain and not to backbone amide transitions.

The F13 side chain contribution in our data is pronounced in comparison to the apelin-13 CD spectrum reported by Fan et al. (*13*). This may be in part due to their measurement being performed at ambient temperature since the Phe side chain bands, particularly at 217−220 nm, are somewhat less intense at 35 °C than at 5 °C (Figure 1). The apelin-13 spectrum reported by Fan et al. also shows noise in the ∼190−200 nm region which may have obscured the band that we observe at 197 nm. Beyond these Phe side chain bands, our CD spectroscopy results are in agreement with Fan et al. and imply that the secondary structuring of the apelins is primarily random coil in nature, with characteristic temperature-dependent change in band intensity (*38*). Minor P_{II} structure is observed at 5 °C as a very weak band at ∼223−225 nm (blue-shifted relative to proline-rich PP_{II} at 228−230 *38, 39*) in the F13A-apelin-13 spectrum. This very weak band has a more canonical PP_{II} position and appearance

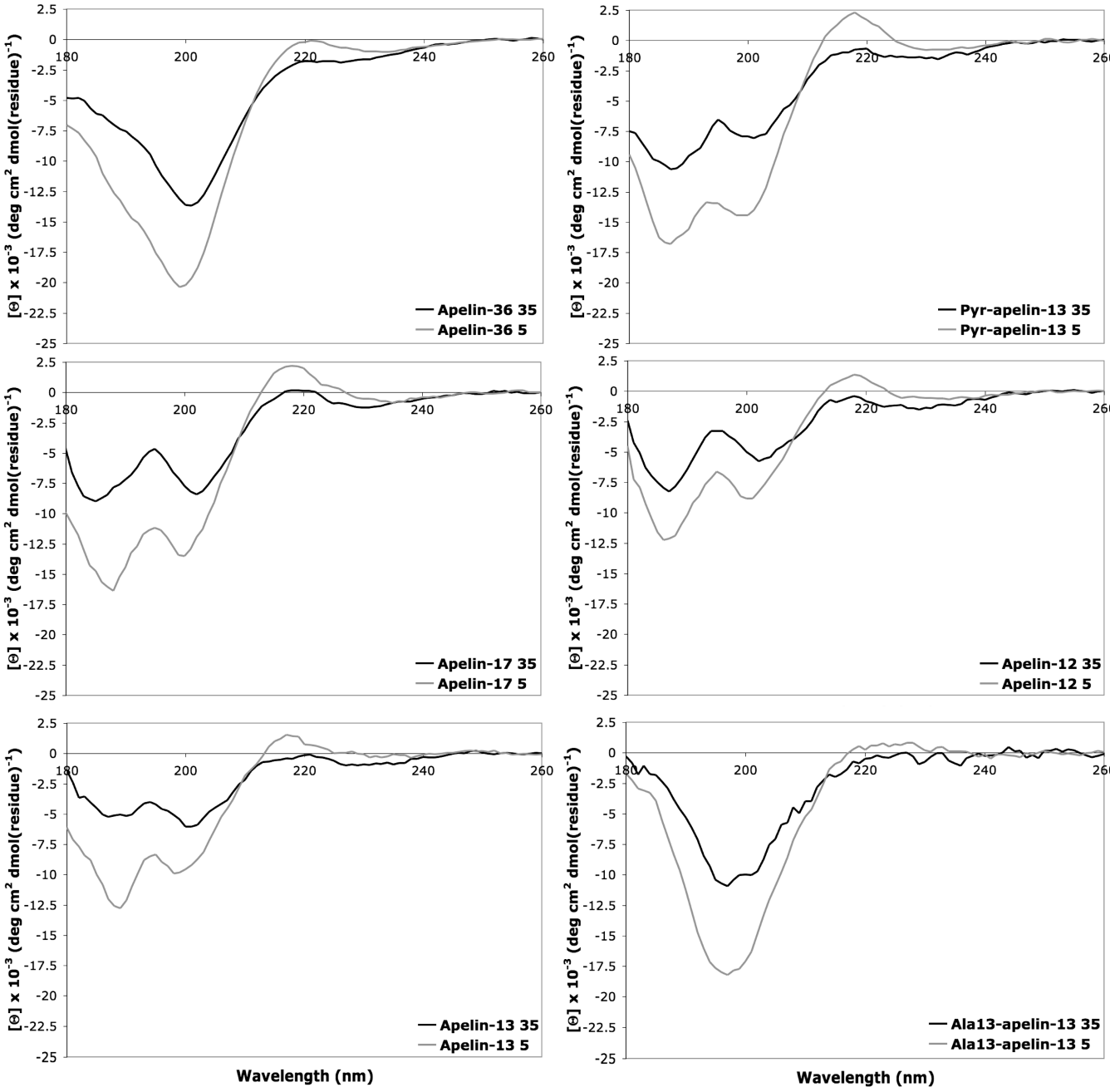

FIGURE 1: Far-ultraviolet circular dichroism spectra of indicated forms of apelin (sequences in Table 1) and for F13A-subsituted apelin-13. Spectropolarimetry (blank subtracted averages of 9 replicates) was performed at 5 °C (gray) and 35 °C (black) in phosphate buffer (20 mM, pH 7.00 ± 0.05) at ~200 μM apelin, with exact concentrations determined by quantitative amino acid analysis for all except Ala13-apelin-13. Note that the reported mean residue ellipticity values [θ] are 3 nm sliding-window averages weighted toward the center wavelength (eq 1); spectra are shown without sliding-window averages in Figure S1 of the Supporting Information. Wavelength values for significant spectral features are tabulated in Table S1 of the Supporting Information.

than the Phe side chain band observed at 217−220 nm in the other forms of apelin observed. This will have a minor convoluting contribution to the shape of the band for a conformationally restricted Phe side chain.

Sequential NMR Assignment of the Apelins. Sequential assignment (*43*) of apelin-17 resonances at 35 and 5 °C was carried out using natural abundance gradient-enhanced $^{13}C-^{1}H$ HSQC and homonuclear TOCSY, NOESY and DQF-COSY experiments. Based on NOE buildup measurements (*43*), a 400 ms mixing time was deemed optimal for the NOESY experiment on apelin-17 (results not shown). Apelin-12, -13, and Pyr-apelin-13 were also sequentially assigned at both temperatures using $^{13}C-^{1}H$ HSQC, TOCSY and ROESY experiments. Nearly complete ^{13}C and ^{1}H atom assignment was possible at both 35 °C and 5−6 °C for all forms of apelin (Table 3).

Chemical shifts of the apelin peptides demonstrate two key features. First, there is no discernible effect of temperature on chemical shift (illustrated for apelin-17 in Figure 2; detailed in Figures S2−S4 of the Supporting Information). Second, the chemical shifts observed for the residues retained between apelin isoforms are extremely similar, excluding the N-terminal portion of the shorter peptides (Figure 2). The shorter apelins are in the molecular weight range where the NOE is minimal (*43*), meaning that NOESY experiments are not viable. ROESY spectra of these peptides

Table 3: Summary of ^{1}H and ^{3}C NMR Assignments That Were Either Not Observable or That Were Ambiguously Assigned for Given Apelin Isoform (Sequences in Table 1)

data set	missing resonance assignments
apelin-12 6 °C	R1-HN,H$^{\eta}$
apelin-12 35 °C	R1-HN,H$^{\eta}$ R3-H$^{\eta}$ K7-H$^{\zeta}$
apelin-13 5 °C	Q1-HN R2-H$^{\varepsilon}$,H$^{\eta a}$ R4-H$^{\varepsilon}$,H$^{\eta a}$ K8-H$^{\zeta}$
apelin-13 35 °C	Q1-HN R2-C$^{\alpha}$,H$^{\eta}$ R4-H$^{\eta}$ H7-H$^{\alpha}$,C$^{\alpha}$ K8-H$^{\zeta}$ M11-C$^{\alpha}$
Pyr-apelin-13 6 °C	Q1-HN R4-H$^{\eta}$
Pyr-apelin-13 35 °C	Q1-HN R2-H$^{\eta}$ R4-H$^{\eta}$ H7-H$^{\alpha}$,C$^{\alpha}$ K8-H$^{\zeta}$
apelin-17 5 °C conformer A	K1-HN,H$^{\zeta}$ F2-H$^{\varepsilon}$,C$^{\delta}$,C$^{\varepsilon}$ R3-H$^{\eta a}$ R4-H$^{\eta a}$ R6-H$^{\eta a}$ R8-H$^{\eta a}$ F17-H$^{\varepsilon}$,C$^{\varepsilon}$
apelin-17 5 °C conformer B	K1-HN,H$^{\zeta}$ F2-H$^{\varepsilon}$,C$^{\delta}$,C$^{\varepsilon}$ R3-H$^{\eta a}$ R4-H$^{\eta a}$ R6-H$^{\eta a}$ R8-H$^{\eta a}$ P14-C$^{\delta}$ F17-H$^{\varepsilon}$,C$^{\varepsilon}$,H$^{\zeta}$,C$^{\zeta}$
apelin-17 35 °C	K1-HN,H$^{\zeta}$ R3-H$^{\eta}$ R4-H$^{\eta}$ R6-H$^{\eta}$ R8-H$^{\eta}$ K12-H$^{\zeta}$

[a] Ambiguous assignment (chemical shift assigned, but not uniquely) made for this resonance.

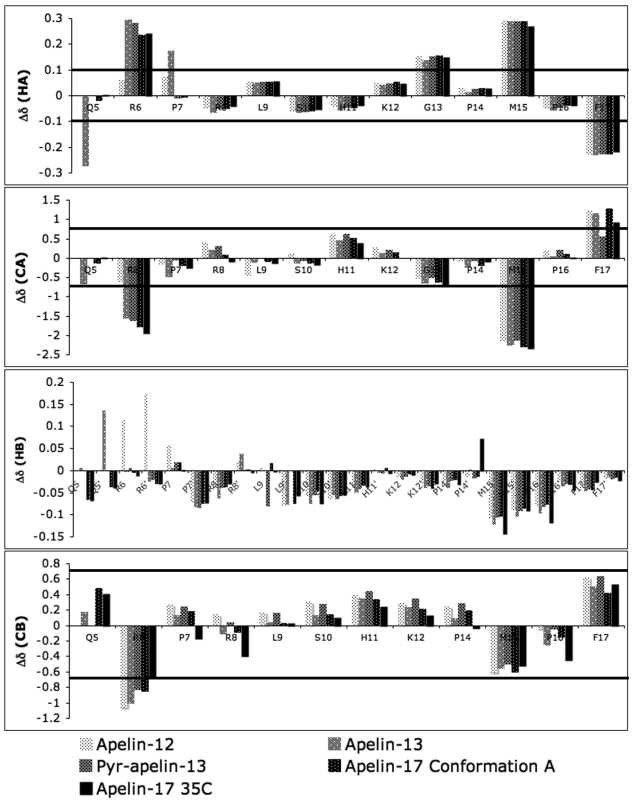

FIGURE 2: Secondary chemical shifts ((*47*), $\Delta\delta = \delta$(observed) − δ(random coil), based on random coil shifts from Wishart et al. (*45*)) for indicated isoform of apelin (sequences in Table 1) at 5 °C alongside those for apelin-17 at 35 °C. $\Delta\delta$ shown for H$^{\alpha}$, C$^{\alpha}$, H$^{\beta}$ and C$^{\beta}$, with degenerate shifts denoted by a prime. The horizontal lines show the values of $\Delta\delta$ identified as significant for secondary structuring by the ^{1}H and ^{3}C chemical shift indices (refs *54* and *55*, respectively); note that C$^{\alpha}$ and C$^{\beta}$ for Pro have identified ranges of ±4 ppm (not shown by horizontal line), unlike the other residues.

are highly overlapped. When combined with convolution of the antiphase *J*-coupled vs dipolar coupled peaks, ROESY assignment was greatly hindered. Hence, full structural analysis and calculation using NOESY assignments and $^3J_{\mathrm{HNH}\alpha}$ couplings was pursued only for apelin-17.

For apelin-17 as well as the shorter apelin peptides examined, slow conformational exchange was apparent at both 5 and 35 °C in the C-terminal region (residues G13−F17 of apelin-17). This gave rise to degenerate spin systems for each of these residues, with a clearly predominant conformer and multiple minor conformers (example shown

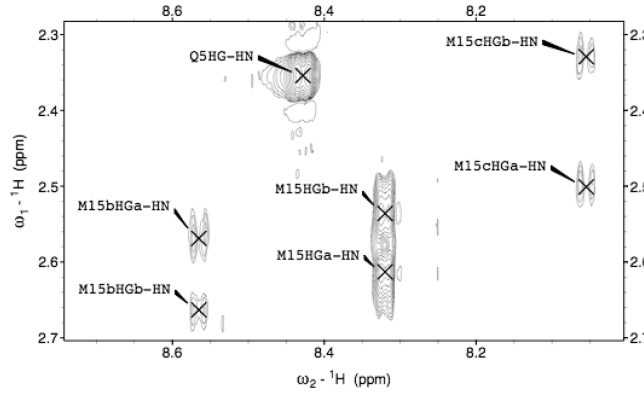

FIGURE 3: The H$^{\beta}$−H$^{\mathrm{N}}$ connectivity region of a ^{1}H−^{1}H total correlation spectroscopy (TOCSY; 60 ms mixing time, DIPSI spin-lock, 800 MHz field strength) experiment acquired for apelin-17 (~3.5 mM peptide in 20 mM $Na^+CD_3COO^-$ buffer at pH 5.00 ± 0.05 prepared in 90% H_2O/10% D_2O with 1 mM NaN_3 and 1 mM DSS) at 35 °C.

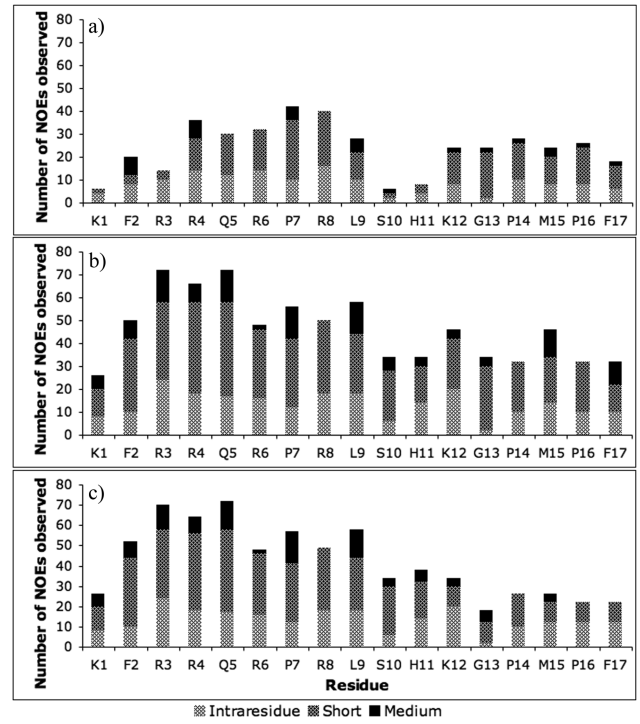

FIGURE 4: A breakdown of nuclear Overhauser effect (NOE) contacts per amino acid residue used to calculate the final ensembles of structures, with short (sequential) and medium ($i - j \leq 4$) NOE interactions shown for apelin-17 at 35 °C (a) and for conformers A and B at 5 °C (shown in (b) and (c), respectively). Note that these plots do not include ambiguous NOEs shown in Table 2.

for M15 in Figure 3). NOE assignments for the major conformer (conformer A) and for the most populated minor conformer (conformer B) were made for apelin-17 at 5 °C, but not at 35 °C due to a lack of observable NOE contacts arising from the lower-intensity degenerate resonances. Each conformer shows distinct sets of sequential and medium ($|i - j| \leq 4$) range NOE contacts over residues 13−17 (26 for conformer A and 10 for conformer B; Figure 4), with K12 showing NOE contacts to G13 of both conformer A and B. Based on peak areas in 1D ^{1}H spectra and volumes in 2D ^{1}H TOCSY spectra, ~20% of the sample is in conformer B and ~80% in conformer A at 5 °C, neglecting the other less populated conformers (estimated at a combined total of <5%

of the ensemble of peptides in solution for all remaining conformers).

In consideration of the nature of conformer A vs conformer B, the fact that *cis*−*trans* peptide bond isomerization is much more favorable for proline than for any other amino acid is critical. To characterize the isomerization state, a characteristic ^{13}C chemical shift difference can be determined using

$$\Delta^{13}C = \delta(C^{\beta}) - \delta(C^{\gamma}) \quad (2)$$

where $\delta(C^{\beta})$ and $\delta(C^{\gamma})$ are the chemical shifts of the indicated ^{13}C nuclei. Work by Schubert et al. shows that $\Delta^{13}C$ is an accurate indicator of the proline N-terminal peptide bond isomerization state (*44*). Using this metric, the N-terminal peptide bonds of P14 and P16 are both in the *trans* form in conformer A ($\Delta^{13}C(P14) = 4.97$, $\Delta^{13}C(P16) = 4.64$) and in the *cis* form in conformer B ($\Delta^{13}C(P14) = 9.53$, $\Delta^{13}C(P16) = 9.81$).

For apelin-17 at 35 °C and conformers A and B at 5 °C, rounds of structure refinement with iterative verification and adjustment of NOE restraints were completed, using the procedure outlined in Experimental Procedures, until the total energies of the structural ensembles converged to a minimum. Table 2 displays a summary of the NOE and DQF-COSY based $^{3}J_{HNH\alpha}$ coupling restraints used as well as average energies and violations of the final 80-member ensembles (80 lowest energy members from 200 calculated structures) of apelin at 5 and 35 °C. Notably, almost double the number of NOE contacts were observed at 5 °C vs 35 °C (Table 2) with NOE contacts spread along the length of the peptide (Figure 4), indicating that structuring is not restricted to a single region. Graphical summaries of NOE restraints (Figure S5 of the Supporting Information) show good connectivity over the length of the peptide without the hallmark features of α-helix or β-sheet structure (*43*).

Structural Features of Apelin-17. Chemical shifts (Figure 2) for apelin-17 at both 35 and 5 °C, as well as for the other three forms of apelin assigned, showed little deviation from random coil values (random coil values of Wishart et al. (*45*) were used). This is not surprising given the strong random coil (and slight PP_{II}) appearance of CD spectra presented both previously in ref *13* and here (Figure 1). Although $^{3}J_{HNH\alpha}$ coupling values were measured and used as restraints (with minimal violations in final structural ensembles, Table 2) at both 35 and 5 °C, most residues still displayed large average deviations for their dihedral angles (Figure S6 of the Supporting Information). Very low dispersion was observed for the dihedrals of the proline residues, as would perhaps be anticipated based on the restriction in conformation imparted by the cyclized side-chain of Pro (*15*). Several type I, II, VI, VIII and many type IV β-turns were detected by Promotif-NMR (*31*) (Table 2). A significant proportion of residues found in "disallowed" regions of the Ramachandran plot (Table 2) is consistent with regions having high type IV β-turn prevalence (*46*).

None of the apelin-17 ensembles demonstrate consistent structuring over the length of the peptide. Rather, a great deal of conformational sampling is apparent. Building on analysis methods detailed previously (*17, 33*), superpositions of each structural ensemble were carried out over 3−6 residue regions starting on each amino acid of apelin-17. Backbone rmsd values and per-residue deviations for each superposed region were then compared to those of a large

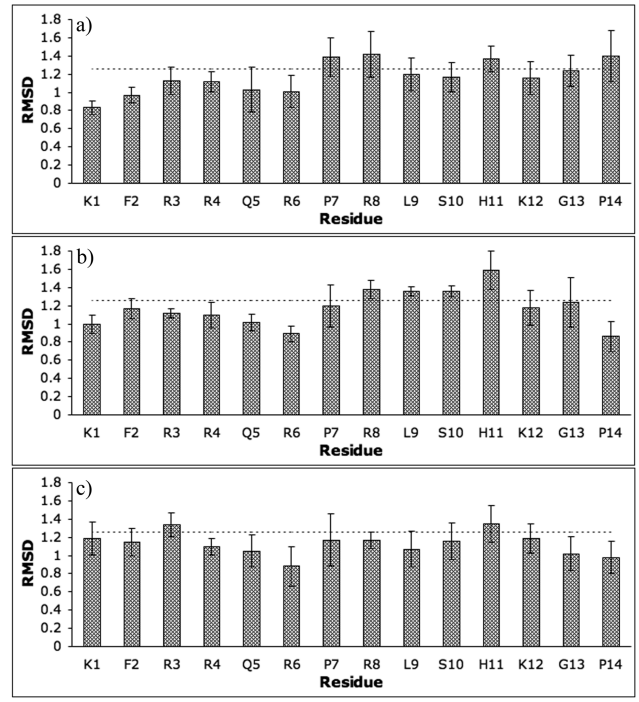

FIGURE 5: Root-mean-square deviation (rmsd) values calculated iteratively for superpositions over 4 residue segments for indicated 80-member NMR-based structural ensembles of (a) apelin-17 at 35 °C, (b) of the primary apelin-17 conformer (conformer A; *trans* peptide bonds at P14 and P16) at 5 °C and (c) of the second most populated apelin-17 conformer (conformer B; *cis* peptide bonds at P14 and P16) at 5 °C. Bars correspond to a superposition starting at the indicated residue with the average deviation for that superposition indicated by the error bar. The average rmsd value of an unconstrained ensemble of 1000 calculated apelin-17 structures superimposed over the 4 residue segments is represented by the dashed line.

(1000 member) apelin-17 ensemble calculated without any NOE or ^{3}J-coupling restraints to determine those segments with rmsds which are significantly better than the unrestrained ensemble (i.e., rmsd of the unrestrained ensemble higher than the rmsd + average deviation of NMR ensemble). This analysis demonstrates clear regions of structural convergence in each ensemble (Figure 5). Note that in some cases, 4 residue superpositions neighboring well-converged regions (F2−Q5 neighboring K1−R4 at 35 °C and Q5−R8 neighboring R9−L9 for conformer A at 5 °C) have lower rmsd than the 1000 member ensemble. However, extension of these two superpositions to 5 residues showed poor structural convergence. We therefore treat only the lower of a pair of neighboring rmsds as a truly converged segment. The neighboring superposition with decreased rmsd is driven to this value through its proximity to the better converged structure. Note that although conformer B at 5 °C does not display a well converged structure over residues K1−R4, unlike apelin-17 in conformer A at 5 °C, the error in rmsd for conformers A and B overlap. This implies that the ensemble of structures for conformer B is just marginally less converged than in conformer A in this region and is likely due to slight differences in the iterative NOE refinement of these two ensembles.

Examination of converged regions defined in this manner (K1−R4, R6−L9 for apelin-17 at 35 °C; and K1−R4, R6−L9 and P14−F17 or G13−F17 for 5 °C data) demonstrated clustering of backbone conformation in each con-

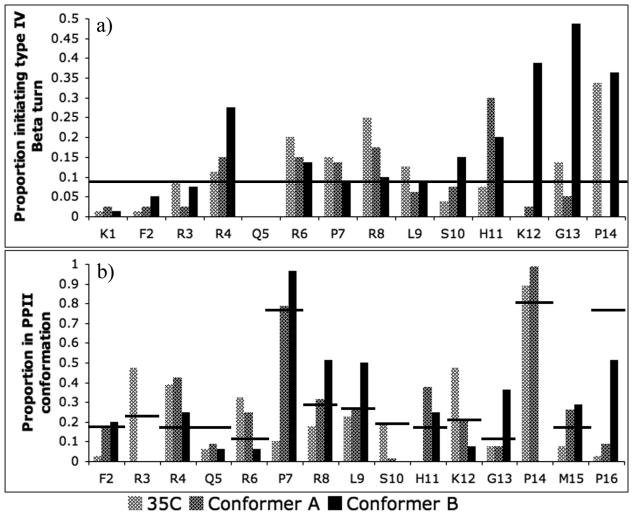

FIGURE 6: (a) Proportion of ensemble members out of the 80-member ensembles with type IV β-turns initiated at the given residue as determined by Promotif-NMR (*31*). Data is shown for all 3 ensembles of apelin-17 structures (one at 35 °C and conformers A and B at 5 °C). The horizontal line represents the average number of type-IV β-turns found in an ensemble of 1000 structures for an unconstrained XPLOR-NIH (*27*) simulated annealing run performed under otherwise identical conditions. (b) Proportion of ensemble members found in polyproline-II (PP_{II}) conformation at given residue, as determined by an in-house tcl/tk script using the PP_{II} (ϕ,ψ) region defined through bioinformatics analysis by Best et al. (*30*) Horizontal lines at each residue show the proportion of that residue found in PP_{II} in the 1000-member unrestrained ensemble.

verged region within each ensemble. Therefore, cluster analysis (*34*) was performed on these regions. In order to consider a clustering result significant for further analysis, the cutoff was imposed that at least two clusters must contain >10% of the ensemble members. According to this cutoff, the G13−F17 region in both conformers A and B of apelin-17 at 5 °C was clustered (colored differently in Figure 7(b, c), magnified in Figure S7 of the Supporting Information). No other structurally converged region contained significant clustering. Details of the clustering and cluster properties are provided in Table S2 of the Supporting Information, with side chain rmsd values of the heavy side chain atoms of these clusters in Figure S8 of the Supporting Information.

In summary, apelin-17 has regions of well-converged structure which undergo conformational sampling relative to each other. Type IV β-turns are prevalent at several residues in comparison to the 1000-member unrestrained apelin-17 ensemble (Figure 6(a); these turn locations are shown graphically in Figure 7(d)). Several residues are also more frequently found in the PP_{II} conformation in the NMR structural ensembles than in the unrestrained ensemble (Figure 6(b); increased proportion of PP_{II} shown in Figure 7(d)). Further complicating the conformational sampling observed between structurally converged regions, the pair of Pro residues near the C-terminus undergo observable *cis*−*trans* isomerization, with two primary conformers at 5 °C being observed where both Pro residues are *trans* (conformer A) or both Pro residues are *cis* (conformer B).

DISCUSSION

Structure of Apelin-17. CD spectra of the all apelin isoforms examined are highly similar and show predominantly random coil character at both 35 and 5 °C (Figures 1 and S1 of the Supporting Information). The chemical shifts for the apelins tend to be close to random coil values (Figure 2 and Figures S2−S4 of the Supporting Information), as would therefore be expected (*47*). Nonetheless, apelin-17 has clear regions of converged structure (Figure 7) identifiable by rmsd analysis of NMR structural ensembles (Figure 5 (*17*)) at K1−R4 (at 35 °C and in conformer A at 5 °C), R6−L9 (both at 35 and 5 °C, increased at 5 °C) and G13−F17 (at 5 °C). Increased apelin-17 structuring upon temperature decrease was somewhat unexpected in light of both NMR chemical shift comparisons and CD spectroscopy. In particular, NMR chemical shifts are minimally different between 35 and 5 °C (Figure 2 and Figures S2−S4 of the Supporting Information), indicative of minimal secondary structuring change. CD spectroscopy (Figures 1 and S1 of the Supporting Information) implies that the only differences in apelin conformation at 5 °C relative to 35 °C are a very slight increase in PP_{II} and, potentially, decreased mobility of the C-terminal Phe resulting in side chain chromophore far-UV CD bands seen in all isoforms except apelin-36. There is no obvious explanation for the lack of bands arising from F36 in apelin-36 CD spectra. Possibilities are that longer-range interactions between the extended N-terminal region of apelin-36 with the C-terminal Phe residue may affect the transitions giving rise to these bands or that there are inherent structural and dynamic differences for this significantly larger peptide form. We intend to examine this discrepancy in future work. Note that a well-defined structuring of the C-terminus at 5 °C would also not normally be anticipated, since polypeptide termini are typically less structured than the remainder of the polypeptide (*43*). The 2 Pro residues in this region assist in providing structuring through reduced conformational freedom due to their cyclic nature (*15*).

The modest increase of PP_{II} structure at 5 °C (i.e., the portion of the CD band at 217−220 nm not due to the C-terminal Phe side chain based on the CD spectrum of F13A-apelin-13) corresponds well with increased proportion of PP_{II} conformation in the structural ensembles at 5 °C vs 35 °C (Table 2; Figure 6(b)). PP_{II} occurrence in all three apelin-17 ensembles is highest at R4, R6−L9, H11 and P14−M15, while S10, which is not converged, shows the least evidence of PP_{II} (Figures 6 and 7). Imposing PP_{II} dihedral restraints (using $-110° \leq \phi \leq -40°$ and $130° \leq \psi \leq 180°$ (*48*)) on a residue-by-residue basis did not reduce mean ensemble energy, suggesting that the PP_{II} content of these regions is persistent but not fixed. Note that the PP_{II} restraints placed upon residues during simulated annealing were stricter than the bioinformatically observed PP_{II} region of Best et al. (*30*) used to detect the presence of PP_{II} in the ensemble of structures (Figure 6(b)). β-turns (mostly type IV) were also frequently observed in the final ensembles (Table 2 and Figure 6(a)). In comparison to β-turn occurrence in the control ensemble of 1000 apelin-17 structures calculated with no restraints, the prevalence of β-turns is highest over the C-terminally converged region and elevated relative to unrestrained apelin-17 in the R6−-R8 region (shown schematically in Figure 7(d) and detailed in Figure 6(b)). Therefore, both PP_{II} and β-turns are prevalent in the most structured regions of apelin-17.

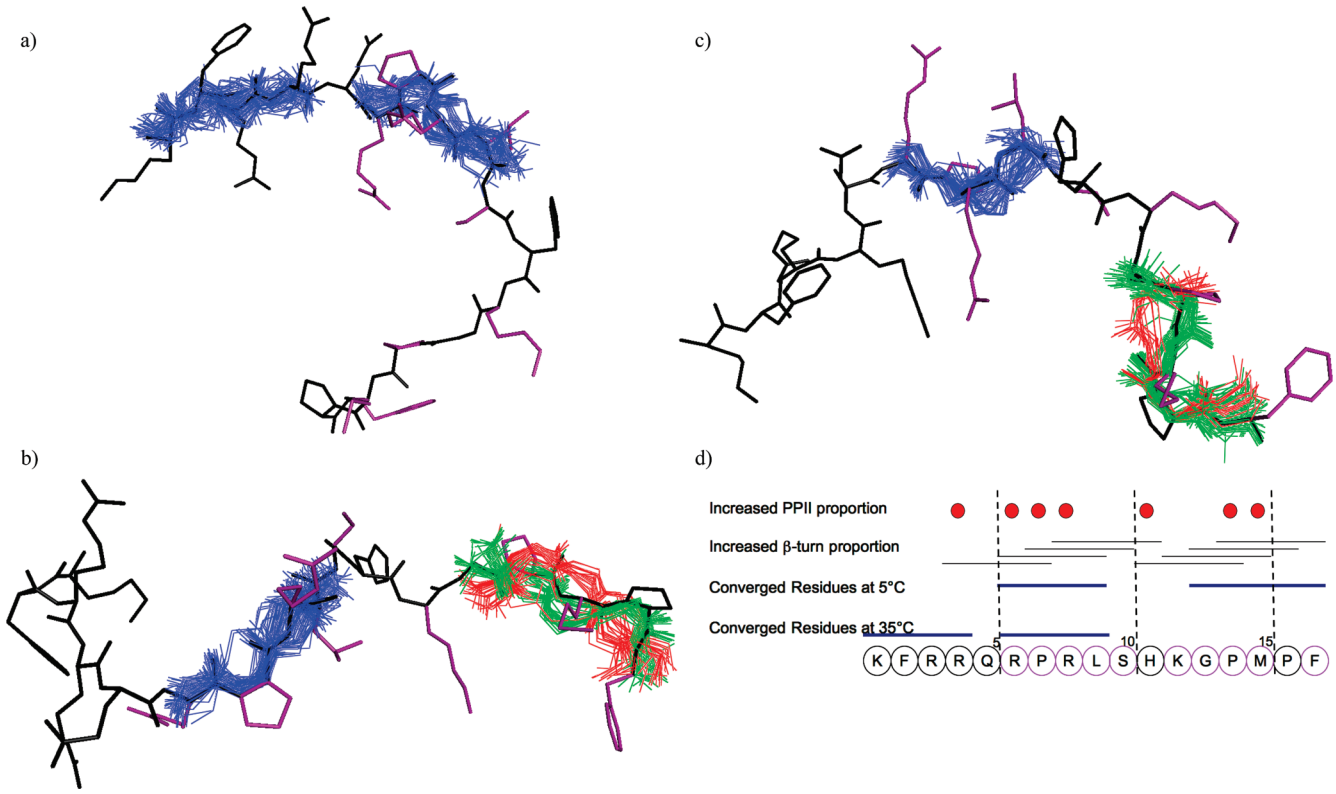

FIGURE 7: Representative structures for apelin-17 structural ensembles (a) at 35 °C, (b) of the primary conformer (conformer A; *trans* peptide bonds at P14 and P16) at 5 °C and (c) of the second most populated conformer (conformer B; *cis* peptide bonds at P14 and P16) at 5 °C are shown in stick form for backbone and side chains. A summary of structural properties is provided in (d) relative to the apelin-17 sequence. For structurally converged regions (identified for each temperature in (d)), the backbones of all 80 ensemble members are shown superposed over the representative structure. Ensemble members are colored by cluster for the C-terminus of (b and c), where major clusters of backbone conformation exist. Functionally critical residues (*11*−*13, 49, 50*) identified by Ala-substitution studies are colored purple, both for side chains in (a−c) and for the circle surrounding the residue in (d). Increased polyproline-II (PP_{II}) and β-turn abundance based on parallel examination of all three ensembles (detailed in Figure 6) are indicated, with all four residues involved in a given β-turn indicated by a bar covering those residues.

The striking similarity of the H^{α}, H^{β}, C^{α} and C^{β} chemical shifts of the shorter apelin peptides to those of apelin-17 (Figure 2 and Figures S2 and S3 of the Supporting Information) suggests that the structuring observed in apelin-17 (Figure 7) is retained in the smaller apelins. This is not surprising, given that all forms of apelin bind to and activate the same GPCR, but is the first experimental evidence that the functionally critical apelin-12 region has a defined structure retained between apelin isoforms. Since PP_{II} has been proposed as an important motif for intermolecular interactions (*16*) and β-turns have been proposed to be a common motif recognized by GPCRs (*14*), the two structurally converged regions of apelin-17 at 5 °C are likely candidates for specific binding to APJ.

Structure−*Function Correlation.* The region of apelin required for binding to and activation of APJ, as demonstrated using truncation mutants, is the C-terminal peptide apelin-12 (Table 1 (*11*)), and the C-terminal Phe is critical according to a number of studies (*12, 49, 50*). Ala-scanning mutagenesis on apelin-13 was published almost simultaneously by two groups (*12, 13*) (also discussed in ref *51*). The residues in apelin (discussed here with apelin-17 numbering) critical for binding and activation of APJ are highlighted in Figure 7(d). Our structural results provide a new context for these mutagenesis studies. Residues in the structurally defined segments at 5 °C (Figure 7b,c) correspond very well to the functionally critical regions identified in the literature (purple circles around residues in Figure 7(d) *11*−*13, 49, 50*). In particular, our NMR data support the idea that R6−L9 are functionally important because of the specific backbone structure they adopt at both 5 and 35 °C. Fan et al. found S10 and K12, found here to be in the flexible linker between structured regions (Figure 7), to be functionally important but not critical (*13*). These residues may facilitate interaction between apelin and APJ, without being essential for binding or activation. A specific structuring in this region, not observed here, may also take place once the receptor−ligand complex is formed. Finally, the importance of G13, P14, M15 and F17 is echoed in the extremely well-converged structure over these residues at 5 °C (Figures 5, 7 and clustering details in Table S2 of the Supporting Information and Figures S7 and S8 of the Supporting Information). The highly evident *cis*−*trans* isomerization in this region, with both prolines being either one isomer or the other in each of the two most populated conformers (conformers A and B of apelin-17 at 5 °C), introduces the issue of which *cis*−*trans* isomers are needed for the binding to or activation of APJ by apelin.

The P16 residue is consistently structured in apelin-17 at 5 °C, but was found to be inessential by Fan et al. (*13*), the only study where a P16A substitution has been made. The Pro to Ala substitution would likely be highly perturbing to structure, although it is possible that an Ala substitution allows similar structure to form. It is notable, however, that contrary to other studies (*12, 49, 50*), Fan et al. also did not find the C-terminal Phe to be essential (*13*). This may

represent a difference in the mechanism of APJ response to apelin in the human APJ HEK293 transfected cells produced and tested by Fan et al. (*13*) compared to those of Medhurst et al. (*12*) or the rat APJ transfected CHO cells used by De Mota et al. (*49*). Indeed, Lee et al. report loss of function for F13A-apelin-13 upon administration to rats (*50*). Since the C-terminal Phe was not susceptible to substitution in the study of Fan et al. but was found to be essential in other physiological assays, a P16A mutant tested differently may indeed perturb apelin-APJ binding or activation.

Insights into Receptor−Ligand Interactions. A hypothetical mode of interaction between apelin and APJ is suggested by the differential structuring of apelin-17 at 35 and 5 °C. At 35 °C, apelin may be undergoing conformational selection, similar to that recently observed for ubiquitin (*19*), facilitating specific binding to APJ. This is most likely initiated in the R6−L9 region of apelin, which is well structured at both 35 and 5 °C. All four residues in this region (RPRL) are highly sensitive to Ala substitution and the N-terminal region of APJ identified as critical using both truncation mutants and Ala-scanning mutagenesis by Zhou et al. (*51*) includes 8 acidic residues and only 2 basic residues. Therefore, the cationic R6 and R8 residues, which generally fall on the same face of apelin-17 in the structural ensembles, provide a likely binding target for the N-terminal region of APJ. The L9 side chain, which is solvent exposed in every ensemble member, may act to strengthen the binding of apelin and APJ through a hydrophobic interaction. Furthermore, the reduced entropy of the R6−L9 region in the free peptide arising from its increased structuring relative to the remainder of apelin, even at 35 °C, is likely to provide a decreased entropic penalty for binding of apelin to APJ vs a binding interaction occurring elsewhere in the peptide.

Although our results cannot confirm or deny this mode of binding, the work of Sykes and co-workers (*21, 23*) demonstrates that it is a reasonable hypothesis that the structuring in the R6−L9 region and at the C-terminus of apelin-17 at 5 °C is representative of the apelin−APJ bound state. Initial binding of the R6−L9 region of apelin to APJ would bring the C-terminal region of apelin into proximity with APJ, facilitating its binding. This would fit well with separate binding and activation steps, as proposed for both class A chemokine GPCRs (*52*) and class B GPCRs (*53*). Determination of the active conformation of apelin in this C-terminal region, including the *cis−trans* isomer forms of P14 and P16, will be critical for understanding apelin function and for developing specific targets for therapeutic design. The potential for a two-step interaction between apelin and APJ provides a key structural starting point for detailed structure−function dissection of the apelin−APJ system.

Summary. All five bioactive forms of apelin examined exhibit almost identical CD spectra and chemical shifts at both physiological (35 °C) and low temperature (5−6 °C), indicating similarity in structure between these five forms of apelin. The apelin-17 structures should, therefore, be highly consistent with the other, shorter apelin isoforms. CD spectral analysis was made difficult by an unusual contribution in the far-UV region from the side chain of the C-terminal Phe, accentuated at low temperature, that may be easily mistaken for predominantly PP_{II} conformation. Upon deconvolution of this CD spectral contribution, the apelins all have a primarily random coil appearance. Despite thus random coil character, the R6−L9 region of apelin exhibits nascent structuring at both 35 and 5 °C. Residues G13−F17 show a high degree of structuring at 5 °C, with clustered backbone conformation, correlating well with far-UV CD bands implying conformational restriction at F17. The apelin peptides all also show strong evidence of *cis−trans* isomerization of the Pro residues in the PMPF motif at the C-terminus, with predominant conformers having either both *trans* (∼80%) or both *cis* (∼20%) peptide bonds. Both structured regions correlate very well to functionally critical regions from previous Ala-substitution studies. Although the free state of apelin-17 has now been well characterized, with potential bound-state conformation and mode of binding postulated from the structural results presented here at 5 °C, further experiments examining the apelin-APJ bound state are required to fully describe the binding interactions in this important system.

ACKNOWLEDGMENT

Thanks to Bruce Stewart for technical support; Drs. Stephen Bearne and David Waisman for access to their CD spectopolarimeters; Dr. Barbara Karten for providing access to her refrigerated centrifuge and Dr. Carmichael Wallace to his lyophilizer; Dr. Mostafa Hatam (AAPPTec) for extremely willing and expert technical advice; Dr. Andrew Roger and Daniel Gaston for advice about NEXUS file format and Figtree; and to Drs. Trevor Creamer (University of Kentucky) and Robert Woody (Colorado State University) for helpful discussions. NMR spectroscopy was performed at the Atlantic Region Magnetic Resonance Centre (ARMRC, Halifax, NS) and National High-Field NMR Centre (NANUC, Edmonton, AB). Thanks to Drs. Michael Lumsden and Kathy Robertson at ARMRC and Dr. Ryan McKay at NANUC for support and advice during NMR experiments.

SUPPORTING INFORMATION AVAILABLE

Tables S1−S2 and Figures S1−S8. This material is available free of charge via the Internet at http://pubs.acs.org.

REFERENCES

1. Tatemoto, K., Hosoya, M., Habata, Y., Fujii, R., Kakegawa, T., Zou, M. X., Kawamata, Y., Fukusumi, S., Hinuma, S., Kitada, C., Kurokawa, T., Onda, H., and Fujino, M. (1998) Isolation and characterization of a novel endogenous peptide ligand for the human APJ receptor. *Biochem. Biophys. Res. Commun. 251*, 471–476.
2. O'Dowd, B. F., Heiber, M., Chan, A., Heng, H. H., Tsui, L. C., Kennedy, J. L., Shi, X., Petronis, A., George, S. R., and Nguyen, T. (1993) A human gene that shows identity with the gene encoding the angiotensin receptor is located on chromosome 11. *Gene 136*, 355–360.
3. Szokodi, I., Tavi, P., Foldes, G., Voutilainen-Myllyla, S., Ilves, M., Tokola, H., Pikkarainen, S., Piuhola, J., Rysa, J., Toth, M., and Ruskoaho, H. (2002) Apelin, the novel endogenous ligand of the orphan receptor APJ, regulates cardiac contractility. *Circ. Res. 91*, 434–440.
4. Boucher, J., Masri, B., Daviaud, D., Gesta, S., Guigne, C., Mazzucotelli, A., Castan-Laurell, I., Tack, I., Knibiehler, B., Carpene, C., Audigier, Y., Saulnier-Blache, J. S., and Valet, P. (2005) Apelin, a newly identified adipokine up-regulated by insulin and obesity. *Endocrinology 146*, 1764–1771.
5. Heinonen, M. V., Purhonen, A. K., Miettinen, P., Paakkonen, M., Pirinen, E., Alhava, E., Akerman, K., and Herzig, K. H. (2005) Apelin, orexin-A and leptin plasma levels in morbid obesity and effect of gastric banding. *Regul. Pept. 130*, 7–13.

6. Kleinz, M. J., and Davenport, A. P. (2005) Emerging roles of apelin in biology and medicine. *Pharmacol. Ther. 107*, 198–211.
7. Kalin, R. E., Kretz, M. P., Meyer, A. M., Kispert, A., Heppner, F. L., and Brandli, A. W. (2007) Paracrine and autocrine mechanisms of apelin signaling govern embryonic and tumor angiogenesis. *Dev. Biol. 305*, 599–614.
8. Sorli, S. C., Le Gonidec, S., Knibiehler, B., and Audigier, Y. (2007) Apelin is a potent activator of tumour neoangiogenesis. *Oncogene 26*, 7692–7699.
9. Hashimoto, T., Kihara, M., Imai, N., Yoshida, S. I., Shimoyamada, H., Yasuzaki, H., Ishida, J., Toya, Y., Kiuchi, Y., Hirawa, N., Tamura, K., Yazawa, T., Kitamura, H., Fukamizu, A., and Umemura, S. (2007) Requirement of Apelin-Apelin Receptor System for Oxidative Stress-Linked Atherosclerosis. *Am. J. Pathol. 171*, 1705–1712.
10. Bray, B. L. (2003) Large-scale manufacture of peptide therapeutics by chemical synthesis. *Nat. Rev. Drug Discovery 2*, 587–593.
11. Tatemoto, K., Takayama, K., Zou, M. X., Kumaki, I., Zhang, W., Kumano, K., and Fujimiya, M. (2001) The novel peptide apelin lowers blood pressure via a nitric oxide-dependent mechanism. *Regul. Pept. 99*, 87–92.
12. Medhurst, A. D., Jennings, C. A., Robbins, M. J., Davis, R. P., Ellis, C., Winborn, K. Y., Lawrie, K. W., Hervieu, G., Riley, G., Bolaky, J. E., Herrity, N. C., Murdock, P., and Darker, J. G. (2003) Pharmacological and immunohistochemical characterization of the APJ receptor and its endogenous ligand apelin. *J. Neurochem. 84*, 1162–1172.
13. Fan, X., Zhou, N., Zhang, X., Mukhtar, M., Lu, Z., Fang, J., DuBois, G. C., and Pomerantz, R. J. (2003) Structural and functional study of the apelin-13 peptide, an endogenous ligand of the HIV-1 coreceptor, APJ. *Biochemistry 42*, 10163–10168.
14. Tyndall, J. D., Pfeiffer, B., Abbenante, G., and Fairlie, D. P. (2005) Over one hundred peptide-activated G protein-coupled receptors recognize ligands with turn structure. *Chem. Rev. 105*, 793–826.
15. Rath, A., Davidson, A. R., and Deber, C. M. (2005) The structure of "unstructured" regions in peptides and proteins: role of the polyproline II helix in protein folding and recognition. *Biopolymers 80*, 179–185.
16. Siligardi, G., and Drake, A. F. (1995) The importance of extended conformations and, in particular, the PII conformation for the molecular recognition of peptides. *Biopolymers 37*, 281–292.
17. Rainey, J. K., Fliegel, L., and Sykes, B. D. (2006) Strategies for dealing with conformational sampling in structural calculations of flexible or kinked transmembrane peptides. *Biochem. Cell Biol. 84*, 918–929.
18. Wright, P. E., Dyson, H. J., and Lerner, R. A. (1988) Conformation of peptide fragments of proteins in aqueous solution: implications for initiation of protein folding. *Biochemistry 27*, 7167–7175.
19. Lange, O. F., Lakomek, N.-A., Fares, C., Schroder, G. F., Walter, K. F. A., Becker, S., Meiler, J., Grubmuller, H., Griesinger, C., and de Groot, B. L. (2008) Recognition Dynamics Up to Microseconds Revealed from an RDC-Derived Ubiquitin Ensemble in Solution. *Science 320*, 1471–1475.
20. Brown, J. E., and Klee, W. A. (1971) Helix-coil transition of the isolated amino terminus of ribonuclease. *Biochemistry 10*, 470–476.
21. Booth, V., Slupsky, C. M., Clark-Lewis, I., and Sykes, B. D. (2003) Unmasking ligand binding motifs: identification of a chemokine receptor motif by NMR studies of antagonist peptides. *J. Mol. Biol. 327*, 329–334.
22. Slupsky, C. M., Spyracopoulos, L., Booth, V. K., Sykes, B. D., and Crump, M. P. (2007) Probing nascent structures in peptides using natural abundance 13C NMR relaxation and reduced spectral density mapping. *Proteins 67*, 18–30.
23. Slupsky, C. M., Sykes, D. B., Gay, G. L., and Sykes, B. D. (2001) The HoxB1 hexapeptide is a prefolded domain: implications for the Pbx1/Hox interaction. *Protein Sci. 10*, 1244–1253.
24. Benoiton, N. L. (2006) *Chemistry of Peptide Synthesis*, Taylor & Francis, Boca Raton, FL.
25. Kay, C., Lorthioir, O. E., Parr, N. J., Congreve, M., McKeown, S. C., Scicinski, J. J., and Ley, S. V. (2000) Solid-phase reaction monitoring--chemical derivatization and off-bead analysis. *Biotechnol. Bioeng. 71*, 110–118.
26. Delaglio, F., Grzesiek, S., Vuister, G. W., Zhu, G., Pfeifer, J., and Bax, A. (1995) NMRPipe: a multidimensional spectral processing system based on UNIX pipes. *J Biomol. NMR 6*, 277–293.
27. Schwieters, C. D., Kuszewski, J. J., Tjandra, N., and Marius Clore, G. (2003) The Xplor-NIH NMR molecular structure determination package. *J. Magn. Reson. 160*, 65–73.
28. Ding, J., Rainey, J. K., Xu, C., Sykes, B. D., and Fliegel, L. (2006) Structural and Functional Characterization of Transmembrane Segment VII of the Na+/H+ Exchanger Isoform 1. *J. Biol. Chem. 281*, 29817–29829.
29. Laskowski, R. A., Rullmann, J. A. C., MacArthur, M. W., Kaptein, R., and Thornton, J. M. (1996) AQUA and PROCHECK-NMR: Programs for checking the quality of protein structures solved by NMR. *J Biomol NMR 8*, 477–486.
30. Best, R. B., Buchete, N. V., and Hummer, G. (2008) Are current molecular dynamics force fields too helical? *Biophys. J. 95*, L07–09.
31. Hutchinson, E. G., and Thornton, J. M. (1996) PROMOTIF--A program to identify and analyze structural motifs in proteins. *Protein Sci. 5*, 212–220.
32. Collaborative Computational Project, N. (1994) *Acta Crystallogr., Sect. D: Biol. Crystallogr. 50*, 760–763.
33. Reddy, T., Ding, J., Li, X., Sykes, B. D., Rainey, J. K., and Fliegel, L. (2008) Structural and functional correlation of transmembrane segment IX of the NHE1 isoform of the Na^+/H^+ exchanger. *J. Biol. Chem. 283*, 22018–22030.
34. Diamond, R. (1995) Coordinate-based cluster analysis. *Acta Crystallogr., Sect. D: Biol. Crystallogr. 51*, 127–135.
35. Maddison, D. R., Swofford, D. L., and Maddison, W. P. (1997) NEXUS: An Extensible File Format for Systematic Information. *Syst. Biol. 46*, 590–621.
36. Ulrich, E. L., Akutsu, H., Doreleijers, J. F., Harano, Y., Ioannidis, Y. E., Lin, J., Livny, M., Mading, S., Maziuk, D., Miller, Z., Nakatani, E., Schulte, C. F., Tolmie, D. E., Kent Wenger, R., Yao, H., and Markley, J. L. (2008) BioMagResBank. *Nucleic Acids Res. 36*, D402–408.
37. Greenfield, N. J. (2004) Analysis of circular dichroism data. *Methods Enzymol. 383*, 282–317.
38. Woody, R. W. (1992) Circular dichroism and conformation of unordered polypeptides. *Adv. Biophys. Chem. 2*, 37–79.
39. Chellgren, B. W., and Creamer, T. P. (2004) Short sequences of non-proline residues can adopt the polyproline II helical conformation. *Biochemistry 43*, 5864–5869.
40. Perczel, A., and Hollosi, M. (1996) Turns, in *Circular Dichroism and the Conformational Analysis of Biomolecules* (Fasman, G. D., Ed.) pp 285−380, Plenum Press, New York.
41. Mehlis, B., Rueger, M., Becker, M., Bienert, M., Niedrich, H., and Oehme, P. (1980) Circular dichroism studies of substance P and its C-terminal sequences. CD spectra in aqueous solution and effects of hydrogen ion concentration. *Int. J. Pept. Protein Res. 15*, 20–28.
42. Sreerama, N., Manning, M. C., Powers, M. E., Zhang, J. X., Goldenberg, D. P., and Woody, R. W. (1999) Tyrosine, phenylalanine, and disulfide contributions to the circular dichroism of proteins: circular dichroism spectra of wild-type and mutant bovine pancreatic trypsin inhibitor. *Biochemistry 38*, 10814–10822.
43. Wüthrich, K. (1986) *NMR of proteins and nucleic acids*, Wiley, New York.
44. Schubert, M., Labudde, D., Oschkinat, H., and Schmieder, P. (2002) A software tool for the prediction of Xaa-Pro peptide bond conformations in proteins based on 13C chemical shift statistics. *J. Biomol. NMR 24*, 149–154.
45. Wishart, D., Bigam, C., Holm, A., Hodges, R., and Sykes, B. (1995) 1H, 13C and 15N random coil NMR chemical shifts of the common amino acids. I. Investigations of nearest-neighbor effects. *J. Biomol. NMR 5*, 67–81.
46. Hutchinson, E. G., and Thornton, J. M. (1994) A revised set of potentials for beta-turn formation in proteins. *Protein Sci. 3*, 2207–2216.
47. Wishart, D. S., Sykes, B. D., and Richards, F. M. (1991) Relationship between nuclear magnetic resonance chemical shift and protein secondary structure. *J. Mol. Biol. 222*, 311–333.
48. Vila, J. A., Baldoni, H. A., Ripoll, D. R., Ghosh, A., and Scheraga, H. A. (2004) Polyproline II Helix Conformation in a Proline-Rich Environment: A Theoretical Study. *Biophys. J. 86*, 731–742.
49. De Mota, N., Lenkei, Z., and Llorens-Cortes, C. (2000) Cloning, pharmacological characterization and brain distribution of the rat apelin receptor. *Neuroendocrinology 72*, 400–407.
50. Lee, D. K., Saldivia, V. R., Nguyen, T., Cheng, R., George, S. R., and O'Dowd, B. F. (2005) Modification of the terminal residue of apelin-13 antagonizes its hypotensive action. *Endocrinology 146*, 231–236.

51. Zhou, N., Zhang, X., Fan, X., Argyris, E., Fang, J., Acheampong, E., DuBois, G. C., and Pomerantz, R. J. (2003) The N-terminal domain of APJ, a CNS-based coreceptor for HIV-1, is essential for its receptor function and coreceptor activity. *Virology 317*, 84–94.
52. Clark-Lewis, I., Kim, K. S., Rajarathnam, K., Gong, J. H., Dewald, B., Moser, B., Baggiolini, M., and Sykes, B. D. (1995) Structure-activity relationships of chemokines. *J. Leukocyte Biol. 57*, 703–711.
53. Hoare, S. R. (2005) Mechanisms of peptide and nonpeptide ligand binding to Class B G-protein-coupled receptors. *Drug Discovery Today 10*, 417–427.
54. Wishart, D. S., Sykes, B. D., and Richards, F. M. (1992) The chemical shift index: a fast and simple method for the assignment of protein secondary structure through NMR spectroscopy. *Biochemistry 31*, 1647–1651.
55. Wishart, D. S., and Sykes, B. D. (1994) The 13C chemical-shift index: a simple method for the identification of protein secondary structure using 13C chemical-shift data. *J. Biomol. NMR 4*, 171–180.

BI801864B